Biochimica et Biophysica Acta, 971 (1988) 255–265
Elsevier

BBA 12334

Effective stage in the cell cycle for control of the budding direction of *cdc* mutants of *Saccharomyces cerevisiae* using electric stimulus

Hideaki Matsuoka [a], Satoshi Matsumoto [a], Madoka Kinoshita [a] and Satoshi Yamada [b]

[a] *Department of Industrial Chemistry, Faculty of Technology, Tokyo University of Agriculture and Technology, Tokyo, and* [b] *Institute for Nuclear Study, University of Tokyo, Tokyo (Japan)*

(Received 20 January 1988)
(Revised manuscript received 27 May 1988)

Key words: Electric stimulus; Directional control; Budding direction; *cdc* mutant; (*S. cerevisiae*)

Cell division cycle (*cdc*) mutants of *Saccharomyces cerevisiae* were used to determine the most effective stage for the directional control of cell budding using an electric stimulus. The selected mutants were *cdc* 35 and *cdc* 28, which could be reversibly arrested before spindle pole body satellite formation (SPBSF) and spindle pole body duplication (SPBD), respectively. The budding direction (Θ) was defined so that the direction parallel to that of the electric field was 0°. Considering the symmetry of the experimental conditions, the range of Θ was defined as 0–90°. The electric stimulus applied in the present study was alternating pulses (pulse height, ±15 V; pulse width at half pulse height, 5 μs; frequency; 10 kHz). The peak height of the cross membrane potential was estimated as 472 mV, which was sufficient to induce considerable strain in the cell membrane. In the case of *cdc* 35, the 95% confidence interval (95% CI) of the budding direction was 7–25° when subjected to electric stimulus, while the 95% CI of the budding direction without electric stimulus was 35–57°. In the case of *cdc* 28, 95% CI values of the budding direction with and without electric stimulus were 12–29° and 23–56°, respectively. These results demonstrate that the stage after SPBD is effective for the directional control of yeast cell budding using an electric stimulus. Simultaneously, an electric stimulus reduced the cell budding time of both the *cdc* mutants used. Therefore, the electric stimulus was also effective in promoting cell cycle progression under the present conditions.

Introduction

Vectorial control of cell growth is of biological significance, because it is closely related to the mechanisms of morphological variation and cell differentiation. Recently, a number of research studies have been performed on this subject [1–6]. In a particular case concerning the cell, for instance, it was demonstrated that neurite elongation tended to grow against the gradient of the nerve growth factor concentration [1,2]. This indicates that a particular chemical compounds could guide cell growth direction.

Another important factor which may possibly control vectorial phenomena is the electric field. The intensity of the electric field normally undergone by normal cells in vivo is very low. Experimentally, however, a wider range of electric field can be applied to various cells and we present

Abbreviations: CI, confidence interval; SPBSF, spindle pole body satellite formation; SPBD, spindle pole body duplication.

Correspondence, H. Matsuoka, Faculty of Technology, Tokyo University of Agriculture and Technology, 2-24-16, Nakamachi, Koganei, Tokyo 184, Japan.

results which offer a potential experimental control mechanism of cell growth.

In comparison with chemical reagents, the electric field is more commodious. The electric field can be defined by the following parameters: intensity, time span and location at which electric stimulus will be concentrated. These parameters are more flexible and thus vectorial control can be more easily accomplished using the electric field than with chemical reagents.

It is well known that most biological systems are composed of inter- of intracellular membranes which are electrically insulating barriers. Therefore an externally applied electric potential would be concentrated on the respective membranes and, thus, membrane-associated functions would be preferrentially affected. In fact, a number of studies have provided experimental evidence of the effects of the electric field on biomembrane-associated phenomena, such as dielectric polarization, dielectrophoresis [7], pearl-chain formation [8,9], cell fusion [10–12], and pore formation [13–16].

The budding direction of a wild strain of yeast (*S. cerevisiae*) was investigated previously under electric field on a single-cell level [5]. It was found that the cell budding tended to occur in a direction parallel to the electric field. Since the electric stimulus was an alternating pulsing mode, its effects should have been due to dielectric polarization rather than electrolysis and electrophoresis.

However, before advancing the analysis of its mechanism, it is important to clarify the stage or event during the cell division cycle which is most sensitive to electric stimulus and which determines the budding direction. For this purpose, the cell division cycle (*cdc*) mutants of *S. cerevisiae* are very useful materials. The *cdc* mutants can be arrested at specific stages of the cell cycle simply by incubation at restrictive temperature (38° C) and can then be released to progress through the cell cycle by cooling (25° C) [17–22].

The G_1 phase of the cell cycle can be roughly divided into three stages; the first stage lasting until the occurrence of events controlled by nutrient limitations or the *cdc* 35 gene, the second lasting until the events controlled by mating pheromone or the *cdc* 28 gene occur and the thrid stage lasting until the events controlled by the *cdc* 4 or *cdc* 7 genes occur. Hereby, the disruption of the G_1 phase is possible by using *cdc* 35 and *cdc* 28 mutants. The most typical events observed in which these mutants were arrested were spindle pole body satellite formation (SPBSF) [18,22] and spindle pole body duplication (SPBD) [18–21], respectively. Spindle pole body satellite is an intracellular site at which the spindle pole body arises [23–25]. After the SPBD, microtubules extend from the spindle pole body. The G_1 phase is followed by the S phase, at an early stage of which the budding emergence occurs.

In the present study, the effects of electric stimulus on the budding direction of these two mutants are investigated. The stage at which the budding direction should be determined under electric field is discussed. As is the mechanism of directional control with electric stimulus.

Materials and Methods

Culture and synchronization of cdc mutants. *cdc* 35 and *cdc* 28 mutants were kindly donated by Dr. T. Ishikawa, University of Tokyo, and Dr. Y. Ohya of the same university, respectively. *cdc* mutants were cultured in YPD medium (yeast extract 1%/polypeptone 2%/glucose 2%) for 15 h at 25° C. After collection, the cells were washed and resuspended in a fresh YPD medium at 25° C. The suspension was divided into 5-ml aliquots and maintained at 25° C in test tubes. 1 aliquot was incubated at 38° C for 2 h before use. This procedure arrested the cells at a stage before SPBSF for *cdc* 35 or SPBD for *cdc* 28 in the G_1 phase. Several microliters of the suspension were transferred into the jacketed vessel filled with YPD medium at 38° C under a microscope, as illustrated in Figs. 1 and 2. One cell became fixed at the tip of a supporting capillary tube (2–3 μm in diameter) with slight suction, within 1–2 min. Then temperature of the medium was lowered to start the cell cycle as described below.

Temperature control of cdc mutant cells. In the present experiments, temperature control was important in order to adjust the starting point of the cell cycle. Since mechanical stirring of YPD medium in the vessel caused detachment of the cell from the supporting capillary tube, the medium was cooled by conduction only using a jacketed vessel as shown in Fig. 1. Initially, the tempera-

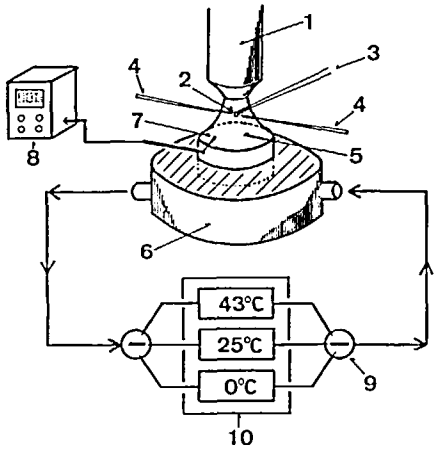

Fig. 1. Experimental set-up for electric stimulation of single cell of the *cdc* mutant of yeast. 1, microscope; 2, yeast cell; 3, supporting capillary tube; 4, microelectrode; 5, YPD medium; 6, jacketed vessel; 7, thermistor; 8, resistance meter; 9, valve; 10, temperature-controlled bath.

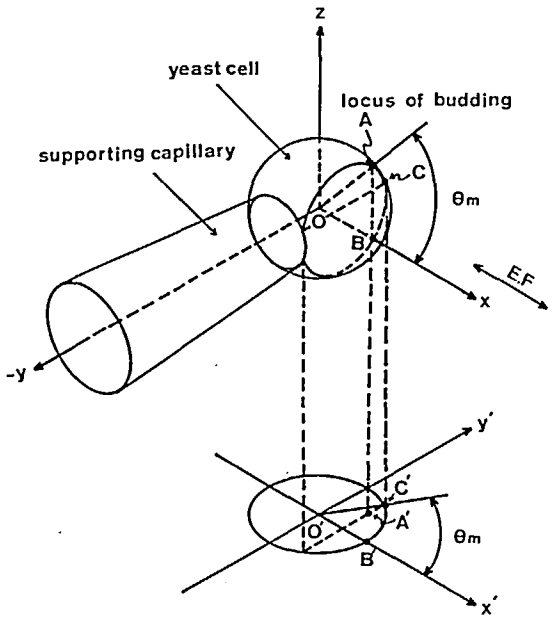

Fig. 2. Determination of budding direction. The budding position (A) was projected to A′ on the x', y'-plane. A was rotated about OB until OA became parallel with the x, y-plane. C indicates the position at which A moved. The angular difference Θ_m ($\angle$BOA) is equal to $\angle$BOC, namely $\angle$B′O′C′ on the x', y'-plane. The budding direction was represented by the normalized value (Θ); $\Theta = \Theta_m$ ($\Theta_m \leq 90°$), $\Theta = 180° - \Theta_m$ ($90° \leq \Theta_m \leq 180°$), $\Theta = \Theta_m - 180°$ ($180° \leq \Theta_m \leq 270°$), $\Theta = 360° - \Theta_m$ ($270° \leq \Theta_m \leq 360°$), where Θ_m is a measured value.

ture of the medium was maintained at 38°C when water, maintained at 43°C, was transferred to the jacket. The temperature was lowered by successive transfer of water at 0°C and water at 25°C. A monitoring thermistor was placed at the middle of the vessel. The temperature at the exact position of the fixed cell (cell position) was monitored simultaneously with another thermistor. In this way, the difference of the time courses of the temperatures at these two positions was calibrated.

Electric stimulation. An electric stimulus was applied with two of microelectrodes. Preparation and handling of microelectrodes were performed as described in Ref. 5. Alternating pulses (pulse height, ±15 V; pulse width at half pulse height, 5 μs; frequency, 10 kHz) was applied with a pulse generator. The intensity and spacial profiles of the peak height of the pulsing electric field were estimated as described in detail in the Appendix. At the cell position, the peak height was estimated as 1.61 kV · cm^{-1}. Assuming that a yeast cell is a single spherical shell with a radius of 2 μm, the peak cross membrane potential value was estimated as 472 mV at $\Theta = 0°$, while its minimum was 0 mV at $\Theta = 90°$.

Determination of the budding direction and budding time. Microscopic observation was continued until budding of the fixed cell with or without electric stimulus was observed. The budding time is defined as the period between the relief of cell cycle arrest ($T = 0$) and the bud emergence. The inverse of the budding time is named the budding tendency. If budding did not occur within 1 h, the cell was discarded.

Contrarily, the effects of the electric stimulus on the arrested cell were checked separately. One of the arrested cells was fixed as described above. The electric stimulus was then applied for 20 min with the temperature maintained at 38°C. Subsequently, the electric stimulus was ceased and the temperature was lowered. Observation continued similarly until budding, was recognized.

The budding direction was determined as illustrated in Fig. 2. The budding position (A) was projected onto a horizontal (x', y') plane. The x-axis corresponds to the direction of the electric field, whose direction was taken as 0°. The angular difference between the budding position and the x-axis is given by Θ_m. Since alternating pulses

were applied, the budding direction is represented by the normalized value (Θ) as defined in the legend to Fig. 2.

Results

The temperature-controlling system

Initially, the temperature at the cell position (Fig. 3, position A) was adjusted to 39–41° C. When water at 0° C was transferred to the jacket, the temperature began to decrease. The temperature profiles around the 35° C were almost the same, independent of the initial temperature. In the same manner, similar profiles were obtained at temperatures around 35° C at position B (the middle of YPD medium).

The temperature at position A decreased more rapidly above 33–34° C than the temperature at position B. This is probably because position A resembled the atmosphere maintained at 25° C.

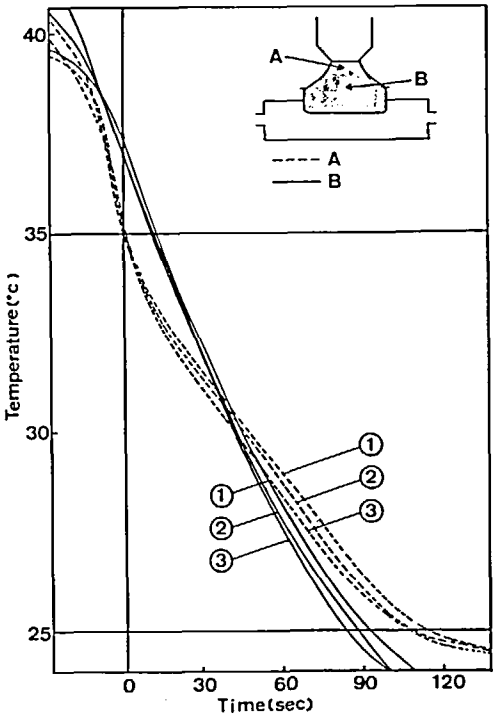

Fig. 3. Comparison of the time courses of temperature at the cell position (A) and the thermistor position (B). Solid lines 1, 2 and 3 (position B) correspond to the broken lines 1, 2 and 3 (position A), respectively.

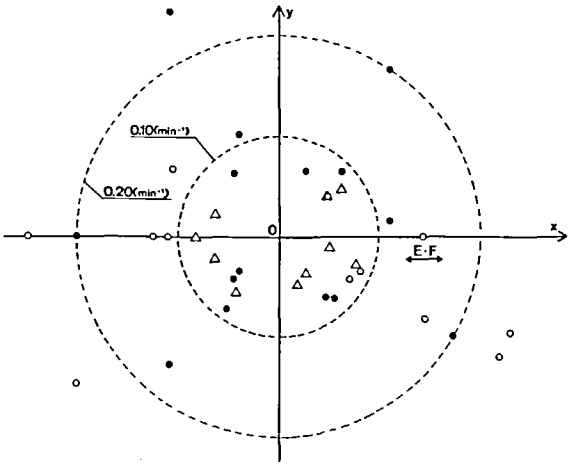

Fig. 4. Budding direction of *cdc* 35 mutant of *S. cerevisiae*. The distance from the origin represents the cell budding tendency (the inverse of the budding time). E·F indicates the electric field. (●), without electric stimulus; (○), with electric stimulus; (△), with electric stimulus during arrest.

Below 32° C, however, the temperature decreased more slowly than that at position B.

The cell cycle of *cdc* mutants begins at a temperature of 35° C, though progress is very slow around this temperature. The time at which the temperature at position A reached 35° C was taken as time zero ($T = 0$), and corresponded to the time at which the temperature at position B reached 37° C. The temperature at position A reached 25° C at about 100–110 s and then reached a steady state level after a slight undershot.

Effect of electric stimulus on the budding direction of cdc 35

Fig. 4 shows results of the budding direction and the cell budding tendency (inverse of the cell budding time). Without electric stimulus, no appreciable dependence was observed in the budding direction, whereas when subjected to the electric field, cell budding seemed to occur in a direction parallel to that of the electric field. This directional dependence is more clearly shown by the histograms of Fig. 5. Without electric stimulus, sample cells budded in the direction 0°–69° and the budding average ($\overline{\Theta}$) for 15 samples was 46°. In sharp contrast, Θ was in the range 0°–40° and $\overline{\Theta}$ was 16° in the presence of an electric stimulus.

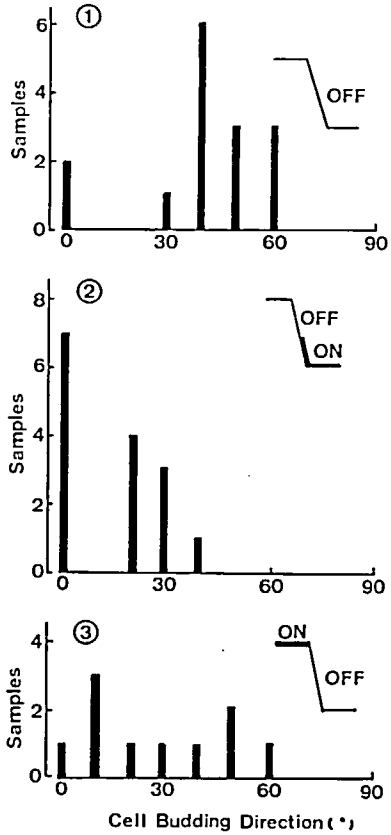

Fig. 5. Histograms of the budding direction of *cdc* 35. The angular division is 10°. On and Off show application and removal of the electric stimulus. The Z-like indication is of the temperature profile obtained from Fig. 3. 1, without an electric stimulus, $\overline{\Theta} = 46°$; 2, with the electric stimulus, $\overline{\Theta} = 16°$; 3, electric stimulus during arrest, $\overline{\Theta} = 33°$. The theoretical value for uniform distribution was $\overline{\Theta} = 45°$.

On the other hand, when the electric stimulus was applied to the arrested cell, $\overline{\Theta}$ was 33°.

The significance of these results was tested based on Student's *t*-distribution and is summarized in Table I. A 95% confidence interval (95% CI) of 35 (2) does not overlap 95% CIs of 35 (2) and UD (2). Therefore, the results of 35 (2) show the effect of the electric stimulus with 95% certainty. On the other hand, the 95% CI of 35 (3) overlaps a small portion of the 95% CI of 35 (2). However, 80% CIs of 35 (2) and 35 (3) no longer overlap. Therefore, 35 (3) can be classified to different results from 35 (2). The electric stimulus is, therefore, effective for budding direction control after SPBSF.

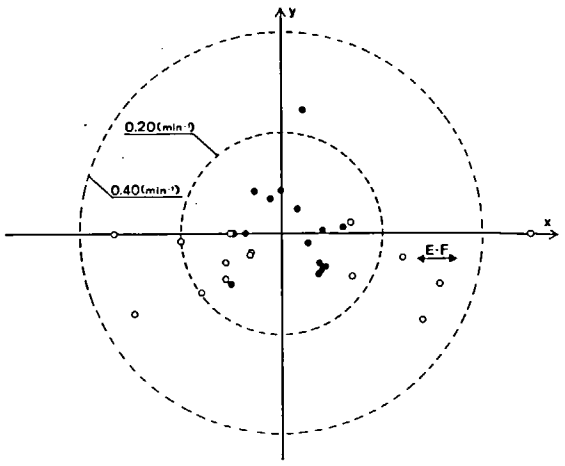

Fig. 6. The budding direction of *cdc* 28 mutant of *S. cerevisiae*. The distance from the origin represents the cell budding tendency. E·F indicates the electric field. (●), without electric stimulus; (○), with electric stimulus.

Effects of an electric stimulus on the cell budding direction of cdc 28

The event of SPBSF is followed by SPBD, spindle pole body separation, and budding emergence in the cell cycle. We, therefore selected *cdc*

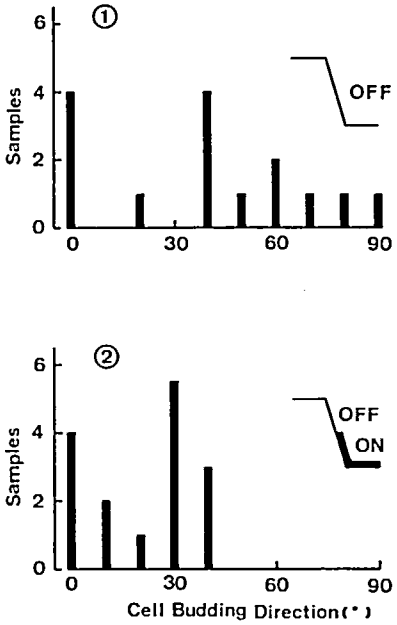

Fig. 7. Histograms of the budding direction of *cdc* 28. The angular division is 10°. 1, without electric stimulus, $\overline{\Theta} = 39°$; 2, with the electric stimulus, $\overline{\Theta} = 21°$.

TABLE I

TEST OF SIGNIFICANCE OF BUDDING DIRECTION AND BUDDING TIME

Student's t-distribution was addopted. 35 (1), 35 (2) and 35 (3) correspond to the results of (●), (○) and (△) in Fig. 4, respectively. 28 (1) and 28 (2) correspond to the results of (●) and (○) in Fig. 6, respectively. UD (1) and UD (2) are theoretical values calculated for uniform distributions of 15 samples and 10 samples, respectively. Confidence intervals are given by the following equation: $\bar{F} - t\sqrt{\Sigma_{i=1}^{n}(F_i-\bar{F})^2/n(n-1)} < F < \bar{F} + t\sqrt{\Sigma_{i=1}^{n}(F_i-\bar{F})^2/n(n-1)}$ where t is the number for Student's t-distribution and n is the number of samples. $\bar{F}$ denotes the average of F. $F=\Theta$ for budding direction and $F=T$ for budding time.

Case	n	Budding direction, $\Theta°$			Budding time, T (min)		
		$\bar{\Theta}$	95%CI	80%CI	$\bar{T}$	95%CI	80%CI
35 (1)	15	46	35–57	39–53	10.1	7.6–12.6	8.6–11.7
35 (2)	15	16	7–25	11–22	7.1	4.9– 9.2	5.7– 8.4
35 (3)	10	33	17–48	23–42	15.5	13.3–17.7	14.2–16.8
28 (1)	15	39	23–56	29–50	10.9	8.9–12.9	9.6–12.1
28 (2)	15	21	12–29	15–26	6.2	4.1– 8.3	4.9– 7.5
UD (1)	15	45	29–61	35–55	–	–	–
UD (2)	10	45	23–67	32–58	–	–	–

28 as the next sample mutant, which could be arrested before SPBD.

Fig. 6 shows the budding directions and the cell budding tendency. As above, the directional dependency is represented in two histograms shown in Fig. 7. In the absence of an electric stimulus, Θ ranged from 0° to 90° and $\bar{\Theta}$ was 40°, whereas in the presence of the electric stimulus, Θ ranged 0° to 40° and $\bar{\Theta}$ was 21°.

As shown in Table I, 80% CI of 28 (2) does not overlap that of 28 (2) nor UD (1). Therefore, the results of 28 (2) show the effect of the electric stimulus with 80% certainty. In other words, the electric stimulus is still effective in controlling the budding direction after SPBD.

Effects of electric stimulus on cell budding time

The cell budding times (T) of *cdc* 35 and *cdc* 28 are summarized in Figs. 8 and 9, respectively. It should be noted that the electric stimulus may reduce the cell budding time. This is supported by the significance test. For *cdc* 35, 95% CI values of T were 7.6–12.6 min and 4.9–9.2 min without and with the electric stimulus, respectively. In the case of *cdc* 28, 95% CI values were 8.9–12.9 min and 4.1–8.3 min without and with the electric stimulus, respectively. Therefore, the effects of the electric stimulus on the cell budding time are significant with 95% certainty. These are the accelerating or promoting effects of cell cycle.

It should be noted, however, that an electric stimulus does not always produce a promotive effect. When the electric stimulus was applied to

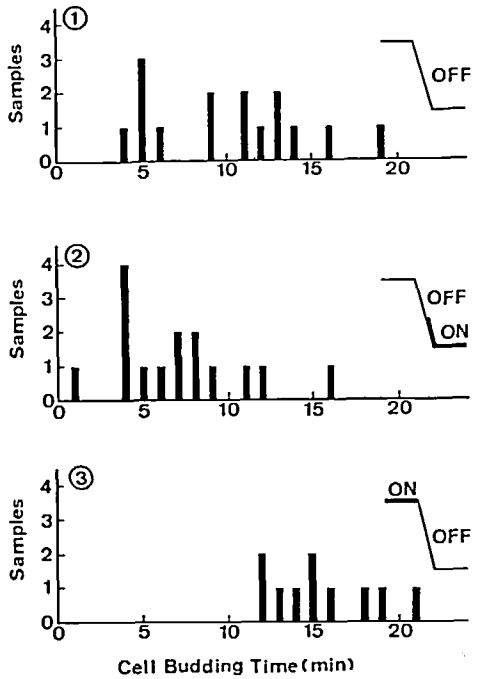

Fig. 8. Histograms of the budding time of *cdc* 35. The time division is 10 min. 1, without electric stimulus, $\bar{T}=10.1$ min; 2, with electric stimulus; $\bar{T}=7.1$ min; 3, with electric stimulus during arrest, $\bar{T}=15.5$ min.

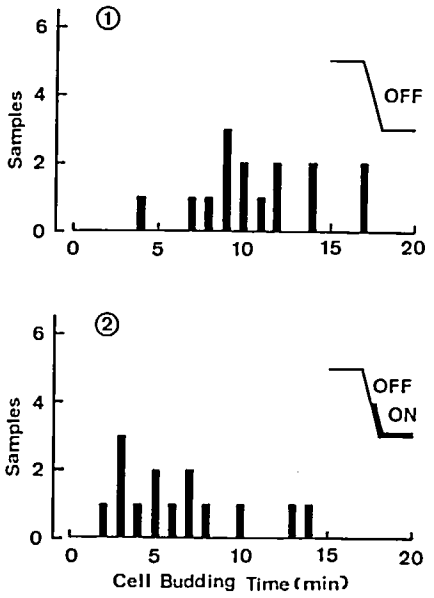

Fig. 9. Histograms of the budding time of *cdc* 28. The time division is 10 min. 1, without electric stimulus; $\bar{T} = 10.9$ min; 2, with electric stimulus, $\bar{T} = 6.2$ min.

arrested cells, it inhibited cell budding as demonstrated with *cdc* 35 (Fig. 8 3). In this case, 95% CI of T was 13.3–17.7 min for 10 samples.

Discussion

The present study demonstrates that the electric stimulus for control of the budding direction is effective after SPBD. During this stage, microtubles begin to grow from the anchorage sites of spindle pole body. Each microtubule undergoes continual addition and polymerization of tubulin molecules at the growing end. Finally, the microtubules protrude at a certain locus of the cell surface, which may become the budding position.

If microtubules grow linearly, like a rigid bar, this indicates that the budding direction has already been determined at the initial stage of its growth. Contrarily, if microtubules are flexible during growth, the budding direction cannot be determined until bud emergence has actually occurred. Though we have no experimental evidence at present, the latter case seems to us more feasible.

The following presents some speculations about which events after SPBD are relevant to directional control by the electric field. The first speculation is based on the flexible properties of growing microtubule as described above. Subjected to an alternating electric field, microtubules would polarize like other dielectric particles and, thus, their free (growing) end would elongate along the electric field. As a result, the budding position would become the locus in a direction parallel to that of the electric field. Considering the field strength of the cell inside (39 $V \cdot cm^{-1}$), however, such a mechanism might not be possible.

A more probable mechanisms would be based on events associated with the mechanical strain of the cell membrane, because the electric field is concentrated on the cell membrane as described in detail in the Appendix. Previous observations show that the breakdown of cell membrane (pore formation or fusion) occurs when the cross membrane potential exceeds 1.0 V [13–16]. According to this criterion, the present experimental condition (maximal $V_{CMP} = 472$ mV) causes considerable mechanical purturbation, though it does not necessarily lead to pore formation. As a result of such mechanical purturbation, a change of ionic permeability is expected to occur. In fact, recent observation of patch clamp experiments [26] has shown that a voltage-sensitive ion channel exists in yeast cell membrane and that it is sensitive to about 50 mV (outside positive) of cross membrane potential [27].

Assuming that some steps of metabolism will be blocked by particular ionic conditions, there is a possibility that such a blocking step will be released by the electric field. From this viewpoint, the role of Ca^{2+} seems very significant. If Ca^{2+} influx is enhanced, it might become a trigger for certain cells to move from the G_0 to G_1 stage. Such effects of the Ca^{2+} influx are supported by experimental results on lymphocyte [28]. Ca^{2+}-dependent transition from the G_1 to the S stage was also demonstrated in cultured cells of rat liver [29].

In the case of *S. cerevisiae*, the significance of Ca^{2+} is also suggested as relevant to the cell cycle control [30–32]. The presence of Ca^{2+}, for example, inhibits the budding of a calcium-sensitive mutant [31]. It is feasible that variation of the Ca^{2+} flux might promote budding by cancelling out the inhibiting effects of Ca^{2+} mentioned above.

However, it is not certain whether these effects on membrane transport systems could be produced in such a site-specific manner as may control the budding direction.

Another possible mechanism is based on the effects on the membrane fusion process. It is well understood that hydrolysis of the cell wall is necessary before budding emergence can occur. In the cytoplasma, there are small vesicles containing cell wall hydrolyzing enzymes such as exo-1,3-β-glucanase [33]. These enzymes have to exit the cell so that they can make contact with the cell wall. It is suggested that this process would be facilitated by fusion of the cell membrane and the vesicle membrane. Such membrane fusion would be promoted by an electric stimulus. Therefore, the cell wall hydrolysis proceeds preferrentially at the locus where the electric field is strongest.

It is also probable that mechanical disturbance might generate a pore or notch in the cell membrane where the growing end of the microtubule could protrude. This means that the budding direction would depend more directly upon mechanical properties of the cell envelope than the intracellular biochemical processes. This assumption does not contradict the former observation that yeast cell budding tended to occur at greater curvature of cell the outline, where mechanical strain would greatest [34].

In conclusion, mechanical properties of the cell membrane are considered an important factor in the speculation of the control mechanism by electric stimulus.

Appendix

Peak value of electric potential between the microelectrode tips (Us)

The electric potential appearing between the tips of microelectrodes (Us) is given by the following equation:

$$Us = \frac{Z_S}{Z_A + Z_B + Z_S} U_o \tag{A-1}$$

where Z_A, Z_B, Z_S are impedances of microelectrodes (A, B) and solution (S), respectively. U_o is the electric potential applied between the microelectrode terminals. Combining Z_A and Z_B to give Z_C, the equation (A-1) can be simplified as follows:

$$U_s = \frac{Z_S}{Z_C + Z_S} U_o \tag{A-2}$$

The peak value of U_s (V_s) is given by the following formula:

$$V_s = \max |U_s| = \frac{|Z_S|}{|Z_C + Z_S|} \cdot \max |U_o| \tag{A-3}$$

The value of $|Z_C + Z_S|$ was obtained by measuring the total impedance of Z_C and $Z_{S,YPD}$ where $Z_{S,YPD}$ is impedance of YPD medium (electric resistivity: $\rho = 2.86 \cdot 10^2\ \Omega \cdot \mathrm{cm}$) between the microelectrode tips, i.e.

$$|Z_C + Z_S| = |Z_C + Z_{S,YPD}| = 65\ \mathrm{M}\ \Omega \tag{A-4}$$

Total impedance obtained by replacing YPD medium by 3 M KCl ($\rho = 2.63\ \Omega \cdot \mathrm{cm}$) corresponded approximately to that of the microelectrodes, because $|Z_C|$ was of the same order as $|Z_{S,YPD}|$ and $|Z_{S,3\,M\,KCl}|$ was sufficiently less than $|Z_{S,YPD}|$. Thus $|Z_S|$ was given as follows:

$$\begin{aligned} |Z_S| &= |Z_T - Z_C| \doteqdot |Z_{T,YPD} - Z_{T,3MKCl}| \\ &\doteqdot |Z_{T,YPD}| - |Z_{T,3MLCl}| \\ &= 65\ \mathrm{M}\ \Omega - 25\ \mathrm{M}\ \Omega \\ &= 40\ \mathrm{M}\ \Omega \end{aligned} \tag{A-5}$$

Substituting 15 V in $\max |U_o|$ of Eqn. (A-3), V_s was estimated as 9.2 V.

Spacial profile of the peak potential

Point electrode analysis. Initially, the electric field between the microelectrodes was calculated based on the point electrode model. Assuming that microelectrodes can be replaced by a point charge, Q and $-Q$ located at P_A (b, 0) and P_B ($-$b, 0), respectively, in the x, y-plane, the electric field strength midway (at $X = 0$) is given as follows:

$$V = \frac{Q}{4\pi\epsilon}\left(\frac{1}{\sqrt{y^2 + (x-b)^2}} - \frac{1}{\sqrt{y^2 + (x+b)^2}}\right) \tag{A-6}$$

$$\left.\frac{\partial V}{\partial x}\right|_{x=0} = \frac{Q}{2\pi\epsilon} \cdot \frac{b}{(y^2+b^2)^{3/2}} \tag{A-7}$$

$$E_0 = \left.\frac{\partial V}{\partial x}\right|_{x=0,y=0} = \frac{Q}{2\pi\epsilon} \cdot \frac{1}{b^2} \tag{A-8}$$

Where ϵ is the dielectric constant of the medium. At the surface of the spheres with radius a ($a \ll b$) situated at P_A (b, 0) and P_B ($-b$, 0), electric potentials are given as follows:

$$V_{PA} = \frac{Q}{4\pi\epsilon}\left(\frac{1}{a} - \frac{1}{2b}\right) \tag{A-9}$$

$$V_{PB} = \frac{-Q}{4\pi\epsilon}\left(\frac{1}{a} - \frac{1}{2b}\right) \tag{A-10}$$

$$V_s = V_{PA} - V_{PB} = \frac{Q}{4\pi\epsilon}\left(\frac{2}{a} - \frac{1}{b}\right) \doteqdot \frac{Q}{4\pi\epsilon} \cdot \frac{2}{a} = \frac{Q}{2\pi\epsilon a} \tag{A-11}$$

From Eqns. A-8 and A-11, E_0 becomes

$$E_o = \frac{aV_s}{b^2} \tag{A-12}$$

Substitution of $V_s = 9.2$ V, $b = 10$ μm and $a = 0.05$ μm gives $E_0 = 46$ V $\cdot$ cm^{-1}. This value is too small in comparison with the result obtained by a more exact analysis given below. This is partly because the equivalent radius of the microelectrode tip was underestimated.

Computer analysis. A computer program 'SUPERFISH' was applied to the analysis of isopotential lines between the microelectrodes. Fig. 10 indicates a model for the microelectrode system. The 'SUPERFISH' was originally developed for the analysis of the spacial profile of the static electric field between axisymmetric electrodes of a linear accelerator [35]. As shown in Fig. 11, the potential gradient at the midpoint between the microelectrodes (E_0) was estimated as 1.61 kV $\cdot$ cm^{-1}.

Cross membrane potential (V_{CMP}) and potential gradient of the cell interior (E_{cell})

Spherical shell model in which the shell interior is an ideal electric conductor. The cross membrane potential (V_{CMP}) was calculated based on the model of the spherical shell, the interior of which is an electric conductor. The following are Laplace's equation with boundary conditions.

$$\Delta V = 0 \tag{A-13}$$

$$\frac{\partial V}{\partial r} = 0 \quad \text{at } r = R + d \tag{A-14}$$

$$V = 0 \quad \text{for } r \leqq R \tag{A-15}$$

$$\frac{\partial V}{\partial x} = -E_o \quad \text{as } r \to \infty \tag{A-16}$$

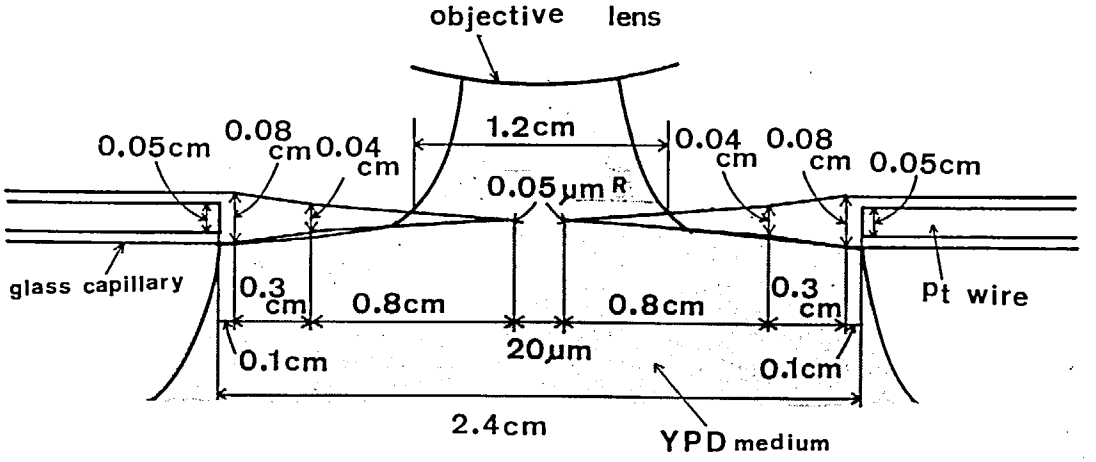

Fig. 10. Dimensions of the microelectrode system. The shaded part represents YPD medium. The surface of the YPD medium was in contact with an object lens of the microscope and pulled up slightly.

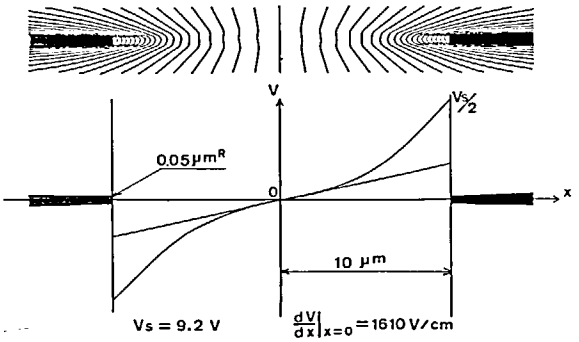

Fig. 11. The electric field between microelectrode tips. Each dimension is shown in Fig. 10.

Solving these equations we obtain:

$$V_{out}(r) = -E_o\left(r + \frac{(R+d)^3}{2r^2}\right)\cos\Theta_m \quad \text{for } R+d \leqq r \tag{A-17}$$

$$V_{in}(r) = 0 \quad \text{for } r \leqq R \tag{A-18}$$

At the outer surface and the inner surface of the shell

$$V_{out}(R+d) = -\tfrac{3}{2}E_0(R+d)\cos\Theta_m \tag{A-19}$$

$$V_{in}(R) = 0 \tag{A-20}$$

$$\therefore V_{CMP} = V_{out}(R+d) - V_{in}(R)$$

$$= -\tfrac{3}{2}E_0(R+d)\cos\Theta_m \tag{A-21}$$

Substitution of $E_0 = 1.61\ \text{kV}\cdot\text{cm}^{-1}$ and $R+d = 2\ \mu\text{m}$ gives $V_{CMP} = 483\cos\Theta$ mV. This value is quite similar to that obtained by the more exact model described below. However, the electric field distribution within the membrane phase cannot be obtained by this simple model.

Spherical shell model in which dielectric constants of respective phases are considered. Considering the dielectric constants of the shell and its interior as well as the external medium, a more exact analysis of electric potential profile was performed. Pauly-Schwan's equation [36] is adopted here.

$$V_{in} = \frac{-9\epsilon_A\epsilon_S E_0 r\cos\Theta m}{(2\epsilon_A+\epsilon_S)(2\epsilon_S+\epsilon_I)+2(\epsilon_A-\epsilon_S)(\epsilon_S-\epsilon_I)w} \tag{A-22}$$

$$V_{shell} = \frac{-3\epsilon_A(2\epsilon_S+\epsilon_I)E_0 r\cos\Theta_m}{(2\epsilon_A+\epsilon_S)(2\epsilon_S+\epsilon_I)+2(\epsilon_A-\epsilon_S)(\epsilon_S-\epsilon_I)w} + \frac{-3\epsilon_A(\epsilon_S-\epsilon_I)E_o R^3\cos\Theta_m}{\{(2\epsilon_A+\epsilon_S)(2\epsilon_S+\epsilon_I)+2(\epsilon_A-\epsilon_S)(\epsilon_S-\epsilon_I)w\}r^2} \tag{A-23}$$

$$V_{out} = -E_o r\cos\theta_m - \left[\{(\epsilon_A-\epsilon_S)(2\epsilon_S+\epsilon_I) + (\epsilon_A+2\epsilon_S)(\epsilon_S-\epsilon_I)v\}E_0(R+d)^3\cos\Theta_m\right] \times\left[\{(2\epsilon_A+\epsilon_S)(2\epsilon_S+\epsilon_I) + 2(\epsilon_A-\epsilon_S)(\epsilon_S-\epsilon_I)w\}r^2\right]^{-1} \tag{A-24}$$

where r is distance from the origin ('O' in Fig. 2). As regards other parameters, the following values were assumed referring to the data in Ref. 37: ϵ_A (dielectric constant of YPD medium) = 80; ϵ_S (dielectric constant of shell (cell membrane)) = 6.62; ϵ_I (dielectric constant of intracellular matrix) = 50.7; $R+d$ (outer radius of cell) = $2\cdot10^{-4}$ cm; d (cell membrane thickness) = 75 Å; w (volume ratio) = $[R/(R+d)]^3$; E_0 (electric field of cell outside) = 1.61 $\text{kV}\cdot\text{cm}^{-1}$. If $\epsilon_A \gg \epsilon_S$ and $\epsilon_I \gg \epsilon_S$ are assumed, Eqn. A-24 becomes equal to Eqn.

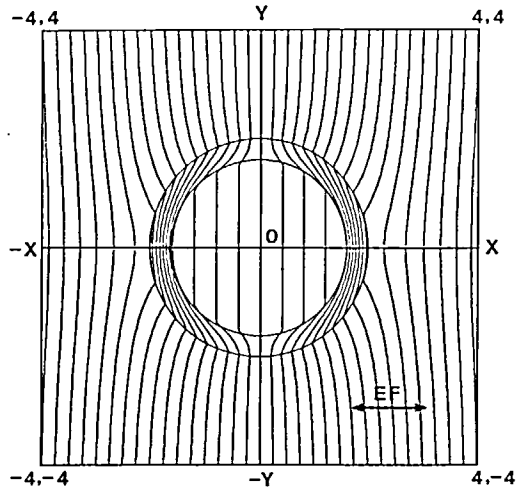

Fig. 12. Isopotential lines in a single shell model under a uniform electric field. The following parameters and boundary conditions were used. Outer diameter, 4 μm; inner diameter, 3.2 μm (the membrane thickness was exaggeratedly increased to help understanding); $E_0 = 1.61\ \text{kV}\cdot\text{cm}^{-1}$; $V(0, y) = 0$ mV; $V(4, \pm4) = -644$ mV; $V(-4, \pm4) = 644$ mV. One division of the isopotential lines corresponds to 40.25 mV.

A-19. On the other hand, the Eqn. A-22 becomes:

$$V_{in} = \frac{-9\epsilon_S E_0 r \cos \Theta_m}{2\epsilon_1(1-w)} \quad \text{(A-25)}$$

V_{CMP} is given by the difference of V_{out} at $r = R + d$ and V_{in} at $r = R$. The peak value of V_{CMP} was calculated as 472 mV at $\Theta = 0°$, while its minimum was 0 mV at $\Theta = 90°$. Within the membrane, the potential profile is given by Eqn. A-23. Electric field inside the cell (E_{cell}) was estimated at 39 $V \cdot cm^{-1}$. Fig. 12 illustrates how the isopotential lines are obtained from Eqns. A-22 to A-24.

Acknowledgments

The authors are grateful to Dr. T. Ishikawa, Dr. Y. Ohya and Dr. Y. Oshumi for kind advice and valuable discussions on *cdc* mutants. The authors also thank Dr. K. Fujibayashi and Dr. N. Koshida for kind comments and valuable discussions of the electric field analysis.

References

1 Gundersen, R.W. and Barret, J.N. (1979) Science 206, 1079–1080.
2 Gundersen, R.W. and Barret, J.N. (1980) J. Cell Biol. 87, 546–554.
3 Jaffe, L.F. and Poo, M-m. (1979) J. Exp. Zool. 209, 115–128.
4 Patel, N.B., Xie, Z-p., Young, S.H. and Poo, M-m. (1985) J. Neurosci. Res. 13, 245–256.
5 Matsuoka, H., Matsumoto, S., Takekawa, Y. and Ai, N. (1986) Biolectrochem. Bioenerg. 16, 235–242.
6 Ferrier, J., Ross, S.M., Kanehisa, J. and Aubin, J.E. (1986) J. Cell Physiol. 129, 283–288.
7 Pohl, H.A. (1978) Dielectrophoresis-The Behavior of Neutral Matter in Nonuniform Electric Field, Cambridge University Press, Cambridge.
8 Zimmermann, U. Vienken, J. and Pilwat, G. (1981) Z. Naturforsch. C: Biosci. 36C, 173–177.
9 Matsuoka, H., Tamiya, E. and Karube, I. (1985) Anal. Chem. 57, 1998–2002.
10 Zimmermann, U. (1982) Biochim. Biophys. Acta 694, 227–277.
11 Lo, M.M.S., Tsong, T.Y., Conrad, M.K., Strittmatter, S.M., Hester, L.D. and Snyder, S.H. (1984) Nature 310, 792–794.
12 Teissie, J., Reynaud, J.A. and Nicolau, C. (1986) Bioelectrochem. Bionerg. 17, 9–15.
13 Coster, H.G.L. and Zimmermann, U. (1975) J. Membr. Biol. 22, 73–90.
14 Kinoshita, K., Jr. and Tsong, T.Y. (1977) Proc. Natl. Acad. Sci. USA 74, 1923–1927.
15 Kinoshita, K., Jr. and Tsong, T.Y. (1977) Biochim. Biophys. Acta 471, 227–242.
16 Karube, I., Tamiya, E. and Matsuoka, H. (1985) FEBS Lett. 182, 90–94.
17 Hartwell, L.H., Culotti, J., Pringle, J.R. and Reid, B.J. (1974) Science 183, 46–51.
18 Hartwell, L.H. (1974) Bacteriol. Rev. 38, 164–198.
19 Pringle, J.R. and Hartwell, L.H. (1981) in The Molecular Biology of Yeast Saccharomyces – Life Cycle and Inheritance (Strathern, J.N., Jones, E.W. and Broach, J.R., eds.), pp. 97–142, Cold Spring Harbor Laboratory, Cold Spring Harbour.
20 Piggott, J.R., Rail, R. and Carter, B.L.A. (1982) Nature 298, 391–393.
21 Moore, S.A. (1984) Exp. Cell Res. 151, 542–556.
22 Plesset, J., Ludwig, J.R., Cox, B.S. and McLaughlin, C.S. (1987) J. Bacteriol. 169, 779–784.
23 Byers, B., Shriver, K. and Goetsch, L. (1978) J. Cell Sci. 30, 331–352.
24 Hyams, J.S. and Borisy, G.G. (1978) J. Cell Biol. 78, 401–414.
25 McIntosh, J.R. (1985) Basic Life Sci. 36, 197–229.
26 Sakman, B. and Neher, E. (1983) Single Channel Recording, Plenum Press, New York.
27 Gustin, M.C., Martinac, B., Saimi, Y., Culbertson, M.R. and Kung, C. (1986) Science 233, 1195–1197.
28 Emilia, G., Torelli, G., Ceccherelli, G., Donelli, A., Ferrari, S., Zucchini, P. and Cadossi, R. (1985) J. Bioelectr. 4, 145–161.
29 Kleine, L.P., Whitfield, J.F. and Boynton, A.L. (1986) J. Cell. Physiol. 129, 303–309.
30 Penman, C.S. and Duffus, J.H. (1975) J. Gen. Microbiol. 90, 76–80.
31 Ohya, Y., Ohsumi, Y. and Anraku, Y. (1984) Mol. Gen. Gent. 193, 389–394.
32 Ohya, Y., Miyamoto, S., Ohsumi, Y. and Anraku, Y. (1986) J. Bacteriol. 165, 25–33.
33 Frey-Wyssling, A. (1971) Proc. Natl. Acad. Sci. USA 68, 636–642.
34 Hayashibe, M. (1977) in NRI Symposia on Modern Biology – Growth and Differentiation in Microorganisms (Ishikawa, T., Maruyama, Y. and Matsumiya, H., eds.), pp. 165–191, University of Tokyo Press, Tokyo.
35 Halbach, K. and Halsinger, R.F. (1976) Part. Accel. 7, 213–222.
36 Pauly, H. and Schwan, H.P. (1959) Z. F. Naturforschung. 14b, 125–131.
37 Asami, K., Hanai, T. and Koizumi, N. (1976) J. Membr. Biol. 28, 169–180.